



Integrated photoelectrochemical energy storage: solar hydrogen generation and supercapacitor

Xinhui Xia^{1,3*}, Jingshan Luo^{1*}, Zhiyuan Zeng², Cao Guan¹, Yongqi Zhang³, Jiangping Tu³, Hua Zhang² & Hong Jin Fan¹

¹Division of Physics and Applied Physics, School of Physical and Mathematical Sciences, Nanyang Technological University, Singapore 637371, Singapore, ²School of Materials Science and Engineering, Nanyang Technological University, Singapore 639798, Singapore, ³State Key Laboratory of Silicon Materials and Department of Materials Science and Engineering, Zhejiang University, Hangzhou 310027, P. R. China.

Received
26 July 2012

Accepted
15 November 2012

Published
14 December 2012

Correspondence and requests for materials should be addressed to H.J.F. (fanhj@ntu.edu.sg)

* These authors contributed equally to this work.

Current solar energy harvest and storage are so far realized by independent technologies (such as solar cell and batteries), by which only a fraction of solar energy is utilized. It is highly desirable to improve the utilization efficiency of solar energy. Here, we construct an integrated photoelectrochemical device with simultaneous supercapacitor and hydrogen evolution functions based on TiO₂/transition metal hydroxides/oxides core/shell nanorod arrays. The feasibility of solar-driven pseudocapacitance is clearly demonstrated, and the charge/discharge is indicated by reversible color changes (photochromism). In such an integrated device, the photogenerated electrons are utilized for H₂ generation and holes for pseudocapacitive charging, so that both the reductive and oxidative energies are captured and converted. Specific capacitances of 482 F g⁻¹ at 0.5 A g⁻¹ and 287 F g⁻¹ at 1 A g⁻¹ are obtained with TiO₂/Ni(OH)₂ nanorod arrays. This study provides a new research strategy for integrated pseudocapacitor and solar energy application.

Solar energy offers a clean, abundant and unlimited energy resource to mankind and provides a green way to fulfil the global demand for carbon-free energy¹. The sunlight provides us with a wide spectrum of applications such as solar heating², photovoltaics³, photoelectrochemical water splitting^{4–6}, photosynthesis⁷, and photocatalysis^{8–10}. However, these solar energy harvest and storage strategies are so far developed as independent technologies. For example, considerable research efforts are being dedicated to TiO₂, but they are mostly specified to only one type of solar energy capture, either the oxidative or reductive energy^{11–18}. More efficient harnessing of the sunlight potential still remains a challenge, which requires new materials or device design.

Among various power sources, supercapacitors have attracted increasing attention over the last decade due to their high power performance, fast recharge capability, and low maintenance cost^{19–21}. While solar-driven supercapacitors are still far from practical applications, the related research is emerging. Recently, Halls *et al.* developed a photogalvanic cells based on lyotropic liquid crystal nanosystems doped by photoactive molecules and showed promise for application as an electrochemical capacitor²². To date, pseudocapacitive metal hydroxides and oxides are being explored for producing supercapacitors with increased specific capacitances and high energy densities^{23–26}. There is little literature on solar-driven supercapacitors based on hydroxides and oxides. This is because almost all the explored pseudocapacitive hydroxides and oxides are not photosensitive under natural sunlight illumination and thus cannot directly capture the solar energy. An effective way is to couple them with photosensitive semiconductor materials, such as TiO₂, WO₃ and MoO₃. The photogenerated electrons and holes, when rationally separated from their exciton state, can drive the reduction and oxidation reactions, respectively²⁷. More specifically, the oxidative energy obtained from light-irradiated semiconductors can be stored in pseudocapacitive materials by electrochemical reactions. Simultaneously, the photoelectrons (reductive energy) can be stored in H₂ via solar light-driven water splitting, or for anti-corrosion²⁸ and bactericidal effects²⁹. Furthermore, most of the pseudocapacitive materials are photochromic, namely, their optical transmission property depends on the charge state. Therefore, this photochromism phenomenon can be used to as an indicator of the solar energy storage within the pseudocapacitive materials.

Based on above considerations, here we report a concept device where both oxidative and reductive energies are effectively utilized by a single electrode. Our concept is illustrated schematically in Fig. 1a. The core components in this device are TiO₂-based core/shell heterostructured nanorod arrays, in which the shell materials are

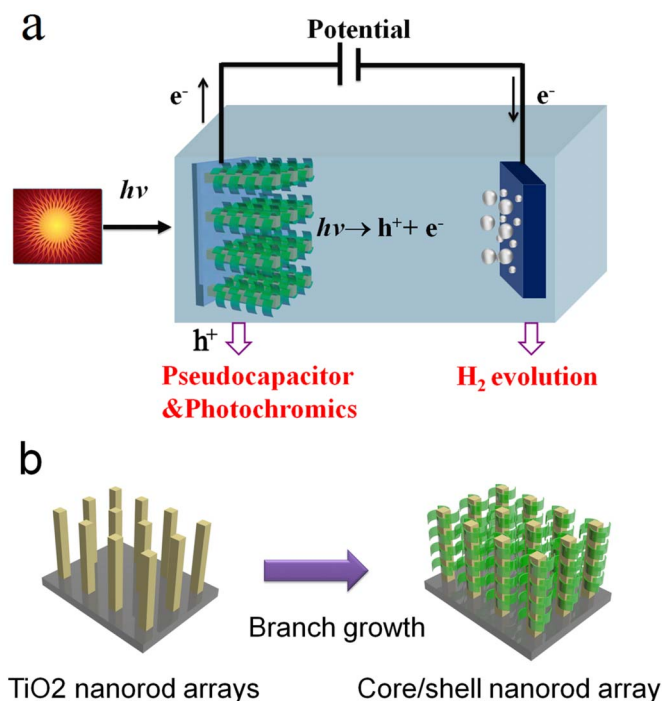
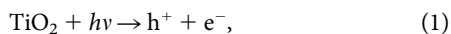


Figure 1 | Design and principle of integrated photoelectrochemical energy storage and photochromic device. (a) Concept of the device based on TiO_2 and transition metal oxides/hydroxides core/shell nanorod arrays. (b) Synthesis of the core/shell nanorod arrays by a two-step solution method: hydrothermal for TiO_2 core, followed by chemical bath deposition or electrodeposition for the branch.

pseudocapacitive transition metal hydroxides or oxides, including $\text{Ni}(\text{OH})_2$, $\text{Co}(\text{OH})_2$ and NiO . The working principle involves two separated processes: photoelectron capture by Pt cathode for H_2 evolution, and hole capture by pseudocapacitive branch materials. In a nutshell, the reactions involved in the integrated photoanode are¹¹:



The corresponding reaction on the Pt electrode is $2\text{H}_2\text{O} + 2e^- \rightarrow \text{H}_2 + 2\text{OH}^-$. Therefore, with this new strategy, it is possible to store solar energy electrochemically.

Results

The TiO_2 nanorod arrays are first hydrothermally grown on FTO glass, followed by coating of shell materials by chemical bath deposition or electrodeposition (see schematics in Fig. 1b). Several core/shell nanorods such as $\text{TiO}_2/\text{Ni}(\text{OH})_2$, $\text{TiO}_2/\text{Co}(\text{OH})_2$ and TiO_2/NiO have been realized. The shell layers have a common flake structure rather than being a continuous shell, which is beneficial to achieving high pseudocapacitive charge/discharge rates. The thickness of the shell layer and the TiO_2 nanorod length can be tuned by controlling the reaction time and reagent concentration. The $\text{TiO}_2/\text{Ni}(\text{OH})_2$ system is chosen for the following discussion, and their structural characterization results are shown in Fig. 2. The TiO_2 nanorods have diameters around 100 nm and lengths up to 1.5 μm as shown by scanning electron microscopy (SEM) images in Fig. S1. The quasi-alignment of the TiO_2 nanorods is desirable for the subsequent branch growth of $\text{Ni}(\text{OH})_2$ nanoflakes. The nanoflakes uniformly cover the whole surfaces of TiO_2 nanorods (see Fig. 2a and b). X-ray diffraction (XRD) patterns reveal the presence of the crystalline rutile TiO_2 (JCPDS 88–1175) and $\beta\text{-Ni}(\text{OH})_2$ (14–0117) (Fig. S1e), supported also by energy disperse spectroscopy (EDS) (Fig. S1f) and fourier transform infrared (FTIR) results (Fig. S2). More details

of this core/shell nanorod heterostructure are revealed by the transmission electron microscopy (TEM) images. The TiO_2 nanorods have smooth sides while rough top surfaces (see Fig. S1c and d), and they are single-crystalline rutile phase with the (001) longitudinal orientation (see the SAED pattern in Fig. S1c). The measured lattice spacings of 0.29 and 0.32 nm are in good agreement with the (001) and (110) interplanar distances of rutile TiO_2 (inset in Fig. S1d). For the core/shell nanorods, the uniform coverage of interconnected nanoflakes of ~ 10 nm can be clearly seen (Fig. 2c and d). The SAED pattern of the nanoflakes is characteristic of polycrystalline $\beta\text{-Ni}(\text{OH})_2$ and the lattice fringes with a lattice spacing of ~ 0.27 nm correspond to the (100) planes of $\beta\text{-Ni}(\text{OH})_2$ (Fig. 2e). In addition, the energy dispersive X-ray spectroscopic (EDS) elemental mappings of Ti and Ni (Fig. 2f) also clearly confirm the core/shell nanorod heterostructure. Note that the $\text{TiO}_2/\text{Ni}(\text{OH})_2$ nanorods can be converted into TiO_2/NiO core/shell nanorods upon annealing at 300°C without morphology change (see Fig. S3). With similar synthetic approach, we have also obtained $\text{TiO}_2/\text{Co}(\text{OH})_2$ nanorod arrays with a similar core/shell morphology (see Fig. S4).

To realize the oxidation of pseudocapacitive materials by photo-generated holes, a reasonable potential bias needs to be selected, so that it only activates the separation of the photogenerated charge carriers but does not cause extra electrochemical reactions. Figure 3a shows the cyclic voltammetry (CV) curves of the TiO_2 nanorod and $\text{TiO}_2/\text{Ni}(\text{OH})_2$ core/shell nanorod arrays under the dark condition. The signal of the TiO_2 nanorod array is negligible. For the core/shell array, when the potential is higher than 0.4 V (vs. Ag/AgCl), intrinsic electrochemical reaction of the redox couple $\text{Ni}(\text{OH})_2/\text{NiOOH}$ occurs. Therefore, in order to avoid the interference of this reaction, we select 0.4 V as the potential bias for the purpose of electron-hole pair separation in the photoelectrochemical process (see below).

To characterize the photoelectrochemical property of the integrated anode, linear sweep voltammograms (LSV) are recorded both in the dark and under simulated solar light illumination condition to show the $J-V$ curves (Fig. 3b). The $\text{TiO}_2/\text{Ni}(\text{OH})_2$ nanorod arrays present a current density of 0.45 mA cm^{-2} at 0.4 V (vs. Ag/AgCl), slightly lower than pure TiO_2 nanorod arrays (0.52 mA cm^{-2}). Both samples show negligible dark current signals. This indicates that the core/shell nanorod arrays can effectively separate the photogenerated electron-hole pairs at 0.4 V bias while the intrinsic electrochemical reaction of $\text{Ni}(\text{OH})_2/\text{NiOOH}$ is not triggered. To double check if the potential bias at 0.4 V is reasonable, we further compare the current-time response under different potential biases. The photocurrent under 0.4 V bias under light illumination is higher than those under 0.35 V and 0.3 V (Fig. 3c), implying that a higher potential bias is more effective in separating the photogenerated carriers. Without light illumination, all potential biases produce only negligible currents. Therefore, it is concluded that 0.4 V is an appropriate potential for the $\text{TiO}_2/\text{Ni}(\text{OH})_2$ system.

Under light illumination at 0.4 V bias for 300 s, the oxidation of $\text{Ni}(\text{OH})_2$ to NiOOH by the photogenerated holes can be manifested by a color change from ivory-white to brown dark (see photographs in Fig. 3d). The photochromism phenomenon is revealed also by the diffuse reflectance spectra (see Fig. 3d). After light illumination, the reflectance of the photoanode significantly lowers due to the strong absorbance of NiOOH . The oxidative energy storage is proven by potential-time response under light illumination (Fig. 3e). Without light illumination, the potential of the photoanode is around -0.3 V. With light at 0.4 V bias for 300 s, the potential quickly increases to 0.35 V and approaches 0.4 V. The post-illumination open-circuit potential maintains at around 0.3 V, indicating that part of the oxidative energy has been stored (Fig. 3f). Note that this potential increase has been also demonstrated in Ni/MH batteries that the potential of the nickel hydroxide electrode will increase over 0.3 V when $\text{Ni}(\text{OH})_2$ is electrochemically oxidized. In contrast, under the dark

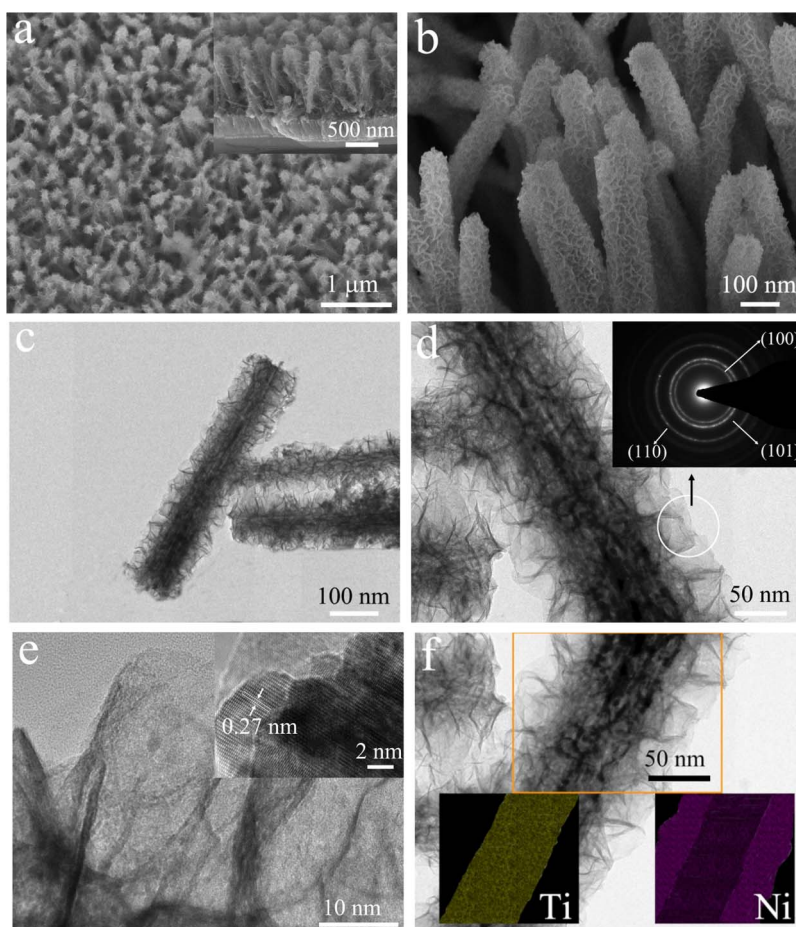


Figure 2 | Morphological and phase characterization of $\text{TiO}_2/\text{Ni}(\text{OH})_2$ core/shell nanorod arrays. (a, b) SEM images at different magnifications. Inset in (a) is a side view of the array. (c, d) TEM images of the heterostructured nanorods (SAED pattern in inset). (e) TEM image of the nanoflake shell (HRTEM image in inset). (f) EDS elemental mappings of Ti and Ni.

condition the potential quickly drops to about -0.15 V (Fig. 3f). This implies no energy has been captured and stored even at the applied potential. The oxidative energy storage and phase change are also confirmed by the X-ray photoelectron spectroscopy (XPS) results (see details in Fig. S5).

The stored oxidative energy is now used for charging a supercapacitor, an electrochemical energy storage device required to provide high power while maintaining its energy density (or specific capacitance) at a high charge/discharge rate. The charge is performed at 0.4 V bias for 300 s under light illumination. The supercapacitor properties are tested by galvanostatic discharge at different current densities. Discharge curves of the $\text{TiO}_2/\text{Ni}(\text{OH})_2$ core/shell nanorod arrays and the corresponding specific capacitance values are shown in Fig. 4a and b, respectively. Although the rate capability is not satisfactory at this stage, the specific capacitance obtained at a low current density (482 F g^{-1} at 0.5 A g^{-1}) by the solar charging is comparable to typical oxide films such as NiO and Co_3O_4 driven by electrical charging^{30–32}. The solar-to-pseudocapacitance efficiency (η) of the $\text{TiO}_2/\text{Ni}(\text{OH})_2$ core/shell nanorod arrays is calculated to be $\sim 0.2\%$ (see experimental in detail). The efficiency is not high mainly due to the relatively low incident-photon-to-carrier conversion efficiency of the TiO_2 host.

Strikingly, Nyquist plots reveal that the electrochemical impedance of the photoanode dramatically decreases to a very low level due to the formation of NiOOH (n-type semiconductor) by photooxidation (Fig. S6a). After discharge, the impedance returns to the high value due to the back reaction to $\text{Ni}(\text{OH})_2$ (p-type semiconductor) (Fig. S6b). Moreover, the overall porous structure, particularly the

flakey branches, can provide large active surface areas (198 m^2 g^{-1} , see Fig. S7) and thus short diffusion paths for both electrons and ions, which is beneficial to high capacitances. The effect of light illumination time on the capacitance is shown in Fig. 4c. One can see that 300 s is a reasonable time to complete the solar charging. In the composite core/shell nanorod arrays, the pure TiO_2 nanorods contribute little to capacitance. All released energy originates from the $\text{NiOOH} \rightarrow \text{Ni}(\text{OH})_2$ conversion with simultaneous reversed color changes from dark to light brown (Fig. 4d). This means the photochromism is reversible in parallel with the charge/discharge cycles. In contrast, without light illumination no discharge behavior can be observed under the same test condition. It is noticed that the $\text{TiO}_2/\text{Ni}(\text{OH})_2$ core/shell nanorod arrays also show color change to light brown under light illumination at open circuit potential without potential bias, but the potential is very low (below -0.2 V). Under this condition, no energy release can be observed even after light illumination for 30 min.

Similar solar electrochemical charging is also demonstrated in TiO_2/NiO (Fig. S8) and $\text{TiO}_2/\text{Co}(\text{OH})_2$ (Fig. S9) core/shell nanorod arrays, except for lower charge separation efficiencies and specific capacitances in these systems compared to $\text{TiO}_2/\text{Ni}(\text{OH})_2$. The TiO_2/NiO core/shell nanorod arrays turn to brown after photooxidation and present a specific capacitance of 133 F g^{-1} at 0.5 A g^{-1} and 56 F g^{-1} at 1 A g^{-1} , respectively. As for the $\text{TiO}_2/\text{Co}(\text{OH})_2$ sample, a specific capacitance of 337 F g^{-1} at 0.5 A g^{-1} is observed with distinct color change from pale green to brown after the charging. The potential bias is dependent on the intrinsic potential of corresponding redox couple. For example, the potential bias for the

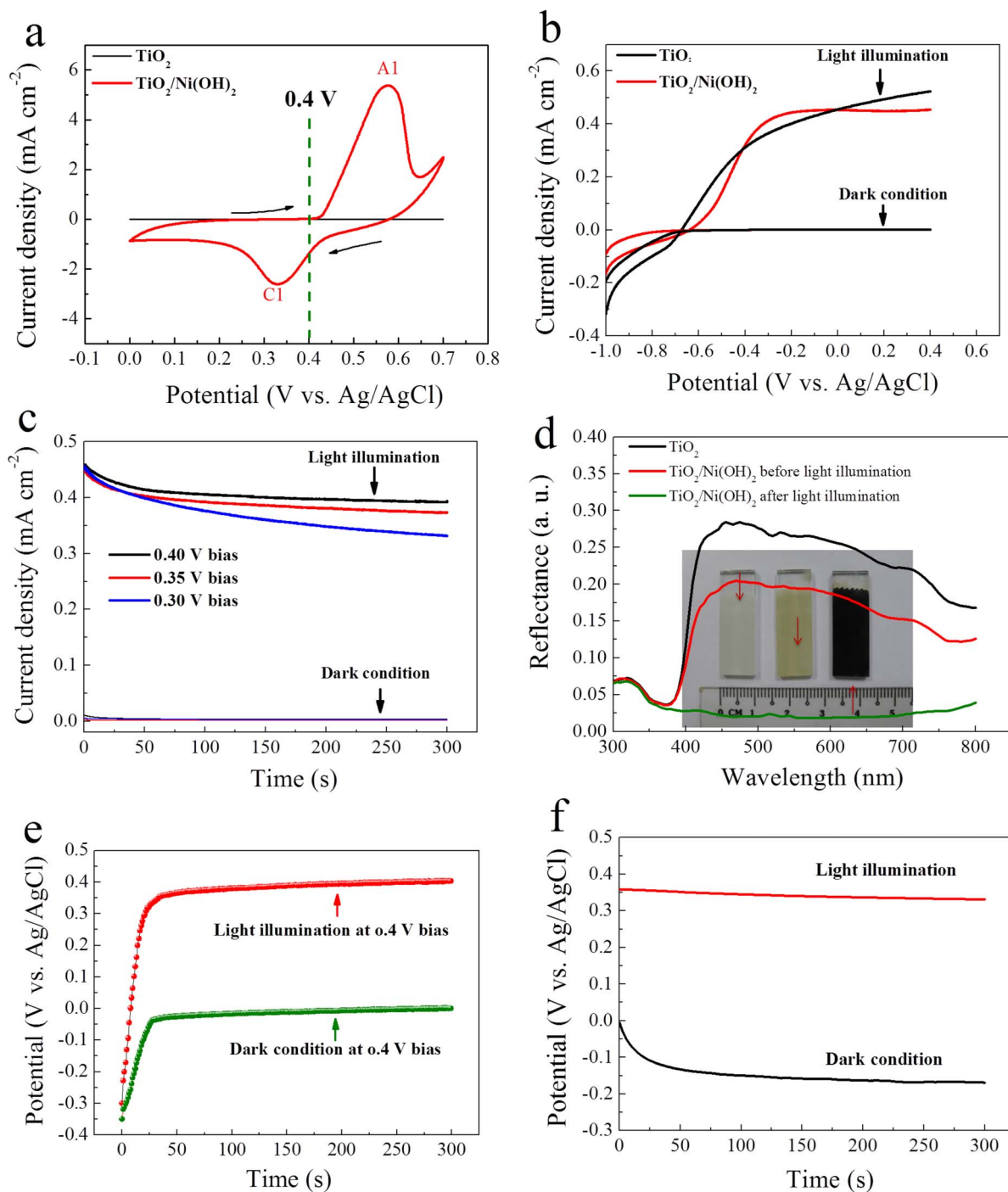


Figure 3 | Photoelectrochemical and photochromic characterizations. (a) CV curves of TiO_2 and $\text{TiO}_2/\text{Ni(OH)}_2$ core/shell nanorod arrays on FTO in the potential region of 0–0.7 V at a scanning rate of 10 mV s^{-1} at the second cycle. (b) $J-V$ curves under dark and simulated solar light illumination. (c) Current-time responses of the core/shell nanorod arrays under different potential biases under dark condition and simulated solar light illumination. (d) Diffuse reflectance spectra before and after simulated solar light illumination (Inset: photographs of the samples). (e) Potential-time responses under dark condition and simulated solar light illumination at 0.4 V bias. (f) Open circuit potential-time responses after 0.4 V bias for 300 s under dark condition and simulated solar light illumination.

$\text{TiO}_2/\text{Co(OH)}_2$ is 0.1 V, lower than those of the $\text{TiO}_2/\text{Ni(OH)}_2$ and TiO_2/NiO (~ 0.4 V). This is understandable as the intrinsic potential of redox couple for $\text{Co(OH)}_2/\text{CoOOH}$ is ~ 0.25 V lower than those of $\text{Ni(OH)}_2/\text{NiOOH}$ and NiO/NiOOH .

Discussion

For a semiconductor to harvest and convert solar energy, it is necessary that, upon light irradiation, the photo-generated electrons and

holes are efficiently dissociated. TiO_2 is an n-type semiconductor in which the electrons in the conduction band are more mobile than holes in the valence band. Hence, the oxidative energy is much more difficult to capture and store than the reductive energy. In our experiment, we utilize the oxidative energy to charge pseudocapacitive materials for supercapacitor application. This design provides several unique features: (i) the pseudocapacitive materials (transition metal hydroxides and oxides) are charged by reacting with

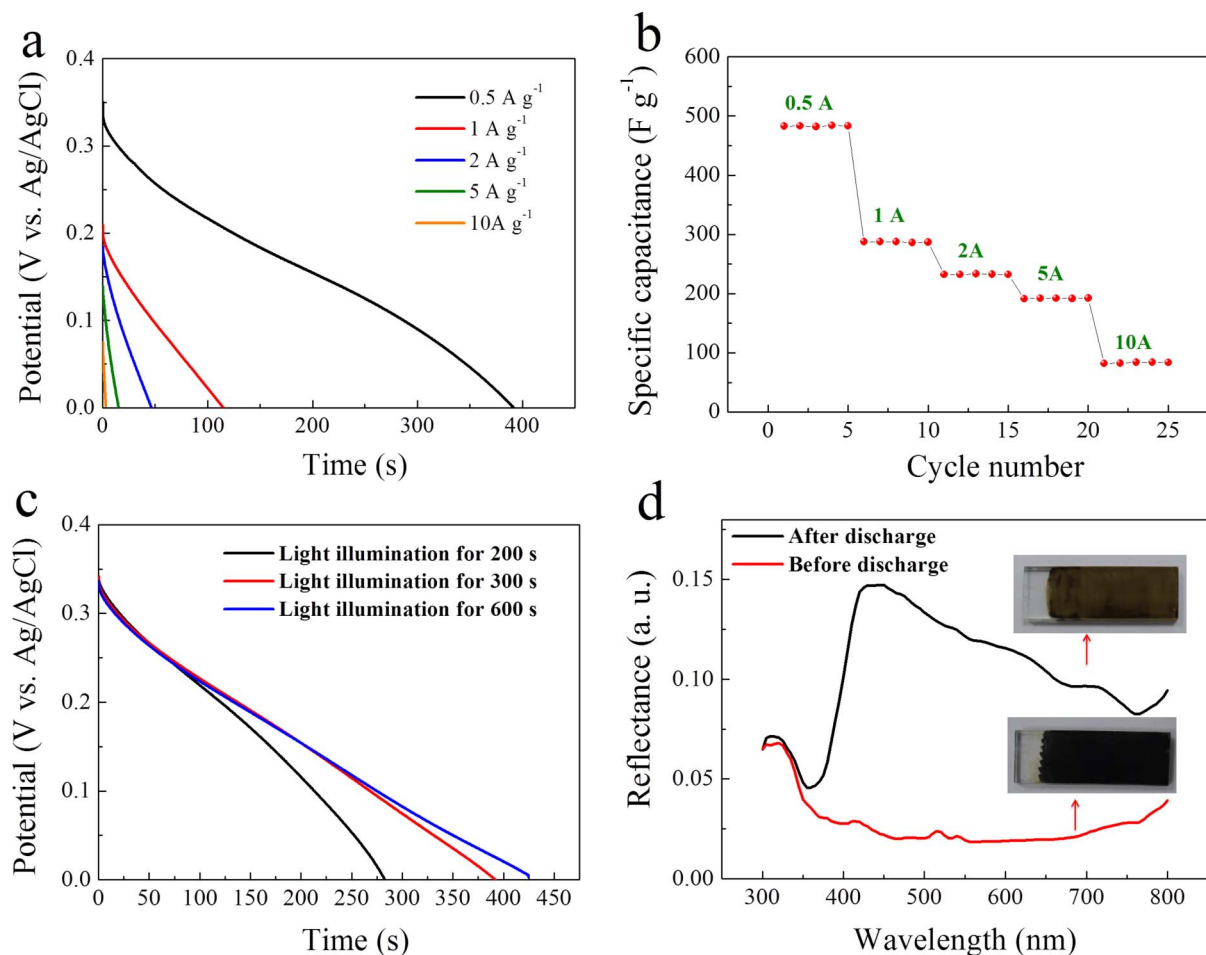


Figure 4 | Pseudocapacitive properties. (a) Discharge curves of $\text{TiO}_2/\text{Ni}(\text{OH})_2$ core/shell nanorod arrays under simulated solar light illumination at 0.4 V bias for 300 s. The current densities from top to bottom correspond to 50, 100, 200, 500, and 1 mA cm^{-2} , respectively. (b) Specific capacitances at various discharge current densities. (c) Discharge curves with different light illumination time at 0.4 V bias. (d) Diffuse reflectance spectra before and after discharge (Inset: photographs of samples).

photogenerated holes; (ii) the pseudocapacitive materials are also photochromics so that the energy storage and release can be monitored by the color change; (iii) the reductive energy is directly used for H_2 evolution at the Pt electrode via sacrificial water splitting. The generated H_2 can be externally stored or used for fuel cells. It is optimistic that such concept could be further improved if appropriate pseudocapacitive materials are selected to couple with TiO_2 (or other solar sensitive semiconductors such as Fe_2O_3 and WO_3). Alternatively, the Pt cathode could be replaced by metal hydrides (MH) such as AB_5 alloys (LaNi₅ type), which are commercial negative materials for Ni/MH rechargeable batteries. In this way, the AB_5 alloys can store the reductive energy by capturing electrons via $2\text{H}_2\text{O} + 2e^- \rightarrow \text{H}_2 + 2\text{OH}^-$; $\text{M} + x/2\text{H}_2 \rightarrow \text{MH}_x$ (M represents metal)³³, so that the charged photoanode and the MH alloys can complete the circuit to release the energy.

In summary, a unique photoelectrochemical device with integrated functions of supercapacitor, hydrogen evolution and photochromics is developed for an improved utilization of solar energy. The feasibility of solar pseudocapacitor charging is demonstrated using TiO_2 -based core/shell nanorod arrays. In this concept, the oxidative energy (photogenerated holes) can be stored by the pseudocapacitive transition metal hydroxides/oxides with simultaneous photochromism as an indicator for energy storage and release. The corresponding reductive energy (photoelectrons) of TiO_2 is directly utilized for H_2 evolution, or potentially by AB_5 -type metal hydrides. As an example, the solar-driven pseudocapacitor based on the $\text{TiO}_2/$

$\text{Ni}(\text{OH})_2$ core/shell nanorod arrays exhibits good specific capacitance values of 482 F g^{-1} at 0.5 A g^{-1} and 287 F g^{-1} at 1 A g^{-1} , respectively. With further optimization, it is optimistic that such integrated devices can have performance comparable to the electrically-charged supercapacitors.

Methods

Synthesis of self-supported $\text{TiO}_2/\text{Ni}(\text{OH})_2$ and TiO_2/NiO core/shell nanorod arrays. Firstly, self-supported TiO_2 nanorod arrays on transparent conductive fluorine-doped tin oxide (FTO) were prepared by a facile hydrothermal synthesis method. In a typical process, the FTO substrates were first cleaned with acetone, ethanol, and deionized water for 5 min, respectively, and then dried by N_2 stream. The precursor was prepared by adding 0.45 mL of titanium butoxide to a well-mixed solution containing 15 mL of HCl and 15 mL of H_2O , and then the whole mixture was stirred for another 10 min until the solution became clear. Afterward, the precursor was poured into a Teflon-liner stainless steel autoclave with the FTO substrates placed at an angle against the wall with the conductive side facing down. Hydrothermal growth was conducted at 150°C for 9 h in an electric oven. Afterward, the FTO substrates were rinsed with deionized water and annealed 450°C for 1 h in ambient air. Then, the self-supported TiO_2 nanorod arrays were used as the scaffold for $\text{Ni}(\text{OH})_2$ and NiO nanoflake growth through a simple chemical bath deposition. In our case, the parameters for chemical bath deposition should be precisely controlled in order to form core/shell structures. TiO_2 nanorod arrays on FTO (masked with polyimide tape to prevent deposition on the back sides) were placed vertically in a 100 ml pyrex beaker. Solution for chemical bath deposition (CBD) was prepared by adding 0.3 ml of aqueous ammonia (25–28%) to the mixture of 70 ml of 0.3 g nickel sulfate and 0.06 g potassium persulfate. Immersing into the stirring CBD solution for 6 min at 25°C , the substrates were taken off and rinsed with distilled water. The samples were annealed at 200°C and 300°C in argon for 1.5 h to form $\text{TiO}_2/\text{Ni}(\text{OH})_2$ and TiO_2/NiO core/shell nanorod arrays, respectively. The load



weight of the TiO₂, Ni(OH)₂ and NiO is approximately 0.75 mg cm⁻², 0.15 mg cm⁻² and 0.11 mg cm⁻², respectively.

Characterization of the core/shell nanorod arrays. The samples were characterized by X-ray diffraction (XRD, RIGAKU D/Max-2550 with Cu K α radiation), field emission scanning electron microscopy (FESEM, FEI SIRION) with energy dispersive spectroscopy, high-resolution transmission electron microscopy (HRTEM, JEOL JEM-2010F), Fourier transform infrared (FTIR) measurements (Perkin Elmer System 2000 FTIR interferometer) and X-ray photoelectron spectroscopy (XPS, PHI 5700). The surface area of the film that scratched from the substrate was determined by BET measurements using a NOVA-1000e surface area analyzer.

Photoelectrochemical and optical measurements. Photoelectrochemical measurements were carried out in a three-electrode configuration with the as-prepared core/shell nanorod arrays as the working electrode, Pt foil as the counter electrode, and saturated Ag/AgCl as the reference electrode. 2 M KOH solution was used as the electrolyte. The intensity of the incident light was calibrated with a standard Si solar cell and controlled at 100 mW cm⁻². The current density versus potential (I–V) curve of the working electrode was carried out by the linear sweep voltammograms with a potentiostat (CHI760D CHI electrochemical workstation) at a scan rate of 10 mV s⁻¹. The reflectance spectra of samples before and after light irradiation were recorded by a Zolix Solar Cell QE/IPCE measurement system equipped with an integrated sphere and a Si diode. After irradiation, the galvanostatic discharge tests of the core/shell nanorod arrays electrodes were performed on a CHI760D with different discharge currents. The specific capacitance is calculated according to the following equation: $C = \frac{I\Delta t}{M\Delta V}$, where C (F g⁻¹) was specific capacitance, I (mA) represented discharge current, and M (mg), ΔV (V) and Δt (sec) designated mass of active materials, potential drop during discharge and total discharge time, respectively. The solar-to-pseudocapacitance efficiency (η) of TiO₂/Ni(OH)₂ core/shell nanorod arrays was calculated according to the equation: $\eta(\%) = W_1/W_2$, where W₁ (J) and W₂ (J) represent the pseudocapacitive energy released from the TiO₂/Ni(OH)₂ core/shell nanorod arrays and radiant energy from the simulated solar light, respectively. W₁ was derived from the discharge curves using the following equation: $W_1 = \frac{1}{2} M_2 C \Delta U^2$, where C (F g⁻¹) is the specific capacitance of the active material, M₂ (mg cm⁻²) was mass of active materials, and ΔU (V) was the voltage range of one sweep segment. W₂ was derived from the following equation: $W_2 = \xi_{light} t$, where ξ_{light} was the irradiance intensity of 100 mW cm⁻², t (s) was the irradiance time.

1. Gratzel, M. Photoelectrochemical cells. *Nature* **414**, 338–344 (2001).
2. Fisch, M. N., Guigas, M. & Dalenback, J. O. A review of large-scale solar heating systems in Europe. *Sol Energy* **63**, 355–366 (1998).
3. Wald, F. V. Efg Crystal-Growth Technology for Low-Cost Terrestrial Photovoltaics - Review and Outlook. *Sol Energ Mater* **23**, 175–182 (1991).
4. Lin, Y. J. *et al.* Semiconductor nanostructure-based photoelectrochemical water splitting: A brief review. *Chem Phys Lett* **507**, 209–215 (2011).
5. Walter, M. G. *et al.* Solar Water Splitting Cells. *Chem Rev* **110**, 6446–6473 (2010).
6. Luo, J. *et al.* Homogeneous Photosensitization of Complex TiO₂ Nanostructures for Efficient Solar Energy Conversion. *Sci Rep* **2**, 451 (2012).
7. Arifin, K., Majlan, E. H., Daud, W. R. W. & Kassim, M. B. Bimetallic complexes in artificial photosynthesis for hydrogen production: A review. *Int J Hydrogen Energy* **37**, 3066–3087 (2012).
8. Kumar, S. G. & Devi, L. G. Review on Modified TiO₂ Photocatalysis under UV/Visible Light: Selected Results and Related Mechanisms on Interfacial Charge Carrier Transfer Dynamics. *J Phys Chem A* **115**, 13211–13241 (2011).
9. Mourao, H. A. J. L., de Mendonca, V. R., Malagutti, A. R. & Ribeiro, C. Nanostructures in Photocatalysis: A Review About Synthesis Strategies of Photocatalysts in Nanometric Size. *Quim Nova* **32**, 2181–2190 (2009).
10. Bard, A. J., Stratmann, M. & Licht, S. (eds.) *Encyclopedia of Electrochemistry: Semiconductor Electrodes and Photoelectrochemistry* Vol. 6. (Wiley, New York; 2002).
11. Kostecki, R., Richardson, T. & McLarnon, D. Photochemical and photoelectrochemical behavior of a novel TiO₂/Ni(OH)₂ electrode. *J Electrochem Soc* **145**, 2380–2385 (1998).
12. Lian, H. Q. *et al.* Oxidative energy storage behavior of a porous nanostructured TiO₂-Ni(OH)₂ bilayer photocatalysis system. *Electrochim Acta* **56**, 2074–2080 (2011).
13. Takahashi, Y. & Tatsuma, T. Oxidative energy storage ability of a TiO₂-Ni(OH)₂ bilayer photocatalyst. *Langmuir* **21**, 12357–12361 (2005).

14. Takahashi, Y. & Tatsuma, T. Remote energy storage in Ni(OH)₂ with TiO₂ photocatalyst. *Phys Chem Chem Phys* **8**, 2716–2719 (2006).
15. Yang, F., Takahashi, Y., Sakai, N. & Tatsuma, T. Visible light driven photocatalysts with oxidative energy storage abilities. *J Mater Chem* **21**, 2288–2293 (2011).
16. Zhang, L. Y. *et al.* UV-Induced Oxidative Energy Storage Behavior of a Novel Nanostructured TiO₂-Ni(OH)₂ Bilayer System. *J Phys Chem C* **115**, 18027–18034 (2011).
17. Zhang, W. K. *et al.* Light energy storage and photoelectrochemical behavior of the titanate nanotube array/Ni(OH)₂ electrode. *Electrochim Acta* **54**, 4760–4763 (2009).
18. Takahashi, Y. & Tatsuma, T. Visible light-induced photocatalysts with reductive energy storage abilities. *Electrochem Commun* **10**, 1404–1407 (2008).
19. Liu, C., Li, F., Ma, L. P. & Cheng, H. M. Advanced Materials for Energy Storage. *Adv Mater* **22**, E28–E62 (2010).
20. Simon, P. & Gogotsi, Y. Materials for electrochemical capacitors. *Nat Mater* **7**, 845–854 (2008).
21. Wang, G. P., Zhang, L. & Zhang, J. J. A review of electrode materials for electrochemical supercapacitors. *Chem Soc Rev* **41**, 797–828 (2012).
22. Halls, J. E. & Wadhawan, J. D. Photogalvanic cells based on lyotropic nanosystems: towards the use of liquid nanotechnology for personalised energy sources. *Energy & Environ Sci* **5**, 6541–6551 (2012).
23. Wang, H. L., Casalongue, H. S., Liang, Y. Y. & Dai, H. J. Ni(OH)₂ Nanoplates Grown on Graphene as Advanced Electrochemical Pseudocapacitor Materials. *J Am Chem Soc* **132**, 7472–7477 (2010).
24. Yuan, L. Y. *et al.* Flexible Solid-State Supercapacitors Based on Carbon Nanoparticles/MnO₂ Nanorods Hybrid Structure. *ACS Nano* **6**, 656–661 (2012).
25. Guan, C. *et al.* Hybrid structure of cobalt monoxide nanowire @ nickel hydroxidenitrate nanoflake aligned on nickel foam for high-rate supercapacitor. *Energy & Environ Sci* **4**, 4496–4499 (2011).
26. Liu, J. P. *et al.* Co₃O₄ Nanowire@MnO₂ Ultrathin Nanosheet Core/Shell Arrays: A New Class of High-Performance Pseudocapacitive Materials. *Adv Mater* **23**, 2076–2081 (2011).
27. Luo, J. *et al.* TiO₂/(CdS, CdSe, CdSeS) Nanorod Heterostructures and Photoelectrochemical Properties. *J Phys Chem C* **116**, 11956–11963 (2012).
28. Tatsuma, T., Saitoh, S., Ohko, Y. & Fujishima, A. TiO₂-WO₃ photoelectrochemical anticorrosion system with an energy storage ability. *Chem Mater* **13**, 2838–2842 (2001).
29. Tatsuma, T., Takeda, S., Saitoh, S., Ohko, Y. & Fujishima, A. Bactericidal effect of an energy storage TiO₂-WO₃ photocatalyst in dark. *Electrochem Commun* **5**, 793–796 (2003).
30. Yuan, Y. F. *et al.* Hierarchically porous Co₃O₄ film with mesoporous walls prepared via liquid crystalline template for supercapacitor application. *Electrochem Commun* **13**, 1123–1126 (2011).
31. Xia, X. H., Tu, J. P., Wang, X. L., Gu, C. D. & Zhao, X. B. Hierarchically porous NiO film grown by chemical bath deposition via a colloidal crystal template as an electrochemical pseudocapacitor material. *J Mater Chem* **21**, 671–679 (2011).
32. Xia, X. H. *et al.* Self-supported hydrothermal synthesized hollow Co₃O₄ nanowire arrays with high supercapacitor capacitance. *J Mater Chem* **21**, 9319–9325 (2011).
33. Sakintuna, B., Lamari-Darkrim, F. & Hirscher, M. Metal hydride materials for solid hydrogen storage: A review. *Int J Hydrogen Energy* **32**, 1121–1140 (2007).

Author contributions

X.H.X., J.S.L. and H.J.F. conceived the experiment. X.H.X. and J.S.L. fabricated the samples. C.G. contributed Fig. 1. X.H.X., J.S.L. and Y.Q.Z. conducted all characterizations. Z.Z.Y. and H.Z. provided the HRTEM images. J.P.T. and Y.Q.Z. provided BET and some SEM figures. X.H.X. and H.J.F. wrote the manuscript. H.J.F. supervised the project. All authors reviewed the manuscript.

Additional information

Supplementary information accompanies this paper at <http://www.nature.com/scientificreports>

Competing financial interests: The authors declare no competing financial interests.

License: This work is licensed under a Creative Commons Attribution-NonCommercial-NoDerivs 3.0 Unported License. To view a copy of this license, visit <http://creativecommons.org/licenses/by-nc-nd/3.0/>

How to cite this article: Xia, X.H. *et al.* Integrated photoelectrochemical energy storage: solar hydrogen generation and supercapacitor. *Sci. Rep.* **2**, 981; DOI:10.1038/srep00981 (2012).